Vidhya et al. Journal of Engineering and Applied Science (2021) 68:32
https://doi.org/10.1186/s44147-021-00034-8

Journal of Engineering and Applied Science

RESEARCH Open Access

Experimental and theoretical investigation of heat transfer characteristics of cylindrical heat pipe using Al_2O_3–SiO_2/W-EG hybrid nanofluids by RSM modeling approach

R. Vidhya[1], T. Balakrishnan[2*] and B. Suresh Kumar[3]

* Correspondence: balacrystalgrowth@gmail.com
[2]Crystal Growth Laboratory, PG and Research Department of Physics, Periyar E.V.R College (Affiliated to Bharathidasan University), Tiruchirappalli, Tamilnadu 620023, India
Full list of author information is available at the end of the article

Abstract

Nanofluids are emerging two-phase thermal fluids that play a vital part in heat exchangers owing to its heat transfer features. Ceramic nanoparticles aluminium oxide (Al_2O_3) and silicon dioxide (SiO_2) were produced by the sol-gel technique. Characterizations have been done through powder X-ray diffraction spectrum and scanning electron microscopy analysis. Subsequently, few volume concentrations (0.0125–0.1%) of hybrid Al_2O_3–SiO_2 nanofluids were formulated via dispersing both ceramic nanoparticles considered at 50:50 ratio into base fluid combination of 60% distilled water (W) with 40% ethylene glycol (EG) using an ultrasonic-assisted two-step method. Thermal resistance besides heat transfer coefficient have been examined with cylindrical mesh heat pipe reveals that the rise of power input decreases the thermal resistance and inversely increases heat transfer coefficient about 5.54% and 43.16% respectively. Response surface methodology (RSM) has been employed for the investigation of heat pipe experimental data. The significant factors on the various convective heat transfer mechanisms have been identified using the analysis of variance (ANOVA) tool. Finally, the empirical models were developed to forecast the heat transfer mechanisms by regression analysis and validated with experimental data which exposed the models have the best agreement with experimental results.

Keywords: Nanofluid, Heat pipe, Heat transfer enhancement, ANOVA, Response surface methodology

Introduction

Nanofluid is an efficient working medium for heat transfer applications in automobile industries, solar collectors, air conditioning, nuclear reactors, microelectronics, computers, and cooling electronic devices [1]. Effectiveness of heat exchanging systems is primarily connected with thermal transport properties of working liquids. Among many heat exchangers, a heat pipe is the modest heat exchanging apparatus that transfers the huge amount of heat energy because of its principle of phase change and

capillary action [2]. Generally, distilled water, engine oils, and ethylene glycol (EG) were used as heat transfer fluids in the heat exchanger, which exhibited less effectiveness in heat, transfer processes [3, 4]. In this regard, many researchers focused their attention on the enrichment of heat transport behavior on conventional working solutions by dissolving the solid nanosized particles (1–100 nm) into conventional fluids, called nanofluids [5–8]. Choi et al. [9] first successfully prepared and analyzed the dispersal of solid nanosized particles into the conventional fluid. He proved the efficiency of nanofluid in thermal conducting features by his work.

Hsin-Tang Chien et al. [10] remained the first one in the evaluation on the efficiency of heat pipes charged with nanofluids. Later, many experimental research works have been conducted by the researchers to assess thermal transferring efficiency on variety of heat pipes with a sort of single component fluids [11–15]. Solomon et al. [16] observed that the heat pipe charged with 0.1% addition of Cu-water nanofluid increases the effective thermal conductivity of the wick structure and enhances the heat transfer capability of the heat pipe by 20%. Akbari et al. [17] analyzed thermal performance and flow regimes of pulsating heat pipe with Graphene/water nanofluid and titania/water nanofluids. They reported that more stable nanofluid has a better thermal performance 70% flow regimes for 70 W. Salehi et al. [18] studied the thermal characteristics of a two-phase closed thermosyphon with Ag/water nanofluid as working fluid and applying a magnetic field. The experimental results showed that the thermal resistance of the thermosyphon decreases with nanoparticle concentration as well as magnetic field strength. Ghanbarpour et al. [19] performed an experiment to investigate the thermal performance of wick structured cylindrical heat pipes using SiC/water nanofluid. Thermal resistance reduction of heat pipes by 11%, 21%, and 30% was observed with SiC nanofluids for 0.35%, 0.7%, and 1.0% volume concentrations. Saeed Zeinali Heris et al. [20] proved that the thermal efficiency of the thermosyphon was improved by analyzing the heat transfer performance of two-phase closed thermosyphon with oxidized CNT/water nanofluids. Zeinali Heris et al. [21] experimentally studied the heat transfer performance of a car radiator with CuO/Ethylene Glycol-Water as a coolant and their results showed that nanofluids clearly enhanced the heat transfer coefficient of about 55% compared to the base fluid.

Previously, researchers examined CuO, Fe_2O_3, Al_2O_3 & SiO_2 [6] single component nanofluids that alter the specific heat capacity, density, thermal conducting feature, as well as viscosity of fluids. Therefore, it is understood that thermophysical properties essentially influences to thermal transferring ability [22, 23]. It is important to indicate that all the combinations of metal-metal, metal-ceramic, and ceramic-ceramic hybrid nanofluids revealed extensive enhancement in thermal conductivity and other thermal characteristics [24–26]. Studies from literatures revealed the thermal transfer features of nanoparticles in aqueous ethylene glycol combination exposed substantial consequences than the common base fluids [25, 27–31]. In our work, the base fluid mixture ratio 60:40 is chosen after several trials. Because, the performance with nanoparticles in W/EG in 60:40 proportion have been intensified significantly in thermophysical properties, stability and thermal conductivity compared to either of the fluids [25, 28, 29].

Among all-ceramic nanoparticles, Al_2O_3 differs from metallic nanoparticles due to its capability of easy incorporation to fluids. Though the thermal conductivity of Al_2O_3 is not significant compared to metal oxides like ZnO and CuO, it is having higher thermal conductivity than the conventional heat transfer fluids [32]. Experimentation on Al_2O_3

nanoparticles exhibited higher hardness, higher insulation, and higher stability. Especially, stable suspensions of aluminium oxide nanoparticles were obtained with the suspended particles inside W/EG solvent [28, 33]. Mashaei et al. [34] analyzed using Al_2O_3/water nanofluid with 0 vol%, 2 vol%, 4 vol%, and 8 vol% in a cylindrical heat pipe which had multiple evaporators. It was found that increase in heat load and concentration of nanoparticles resulted in higher heat transfer coefficient. Keshavarz Moraveji and Razvarz et al. [35] tested alumina/water nanofluid in a sintered wick heat pipe. They found the augmented heat transfer performance for 3% volume concentration of the fluid. Using Al_2O_3/water nanofluids, Noie et al. [36] studied thermal efficiency of a two-phase closed thermosyphon (TPCT). Their results indicated that thermal efficiency improved by increasing the volume fraction of nanoparticles and power. Similarly, SiO_2 nanofluids also shows the enhanced thermal performance. Nabil et al. [25] experimentally tested the thermal conductivity of TiO_2-SiO_2/W-EG nanofluids and observed 22.8% maximum enhancement for 3% volume concentration by increasing the volume concentration and temperature. Using SiO_2–G/EG nanofluid, Akilu et al. [28] established the enhancement in thermal conductivity and viscosity by 26.9% and 1.15 times than the base fluid alone. Yıldız et al. [1] compared the hypothetical and experimental thermal conductivity models and evaluated aqueous-based Al_2O_3/SiO_2 nanofluids efficiency with heat pipe. They observed no significant heat transfer results. Upon deep survey of literature, heat pipe enactment using hybrid nanofluids seems to finite. In addition, there is no such work described in the literature related to the heat transfer analysis in cylindrical mesh heat pipe charged with W/EG based hybrid Al_2O_3–SiO_2 nanofluids.

For better understanding and predicting the experimental process, the models like artificial neural network (ANN) as well as response surface methodology (RSM) would be the powerful tools that are established from the experimental data. Recently, researchers proposed RSM statistical modeling to estimate the various nanofluids' thermal properties based on input parameters such as temperatures and mass volume concentrations. They analyzed the efficiency as well as the performance of heat transfer liquids in detail and illustrated the proposed models were agreed to the experimental data [37–40]. Hemmat et al. [41] designed ANN model on thermal conductivity of Al_2O_3 nanoparticles in W/EG solution with the experimental results. No other work has emphasized the model development using RSM with these two combinations of nanoparticles especially in W/EG mixture. Hence, we focused on the development of the regression models and ANOVA technique with RSM to estimate the correlation between the empirical heat transfer performance data and the models.

This work investigates the heat transfer performance of cylindrical screen mesh heat pipe charged with hybrid W/EG based Al_2O_3–SiO_2 liquids with different volume concentrations for 0%, 0.0125%, 0.025%, 0.05%, 0.075%, and 0.1% at the moderate heat inputs of 30, 60, and 90 W. Response surface methodology and ANOVA tool were employed to investigate the relationship between dependent and independent variables. New regression correlations were established using the experimental results for the assessment of thermal resistance besides heat transfer coefficient that is not noticed in the literature widely.

Methods

All the chemicals used in testing have been purchased from Sigma-Aldrich in the analytical grade and used for experimentation without further purification.

Production of Al_2O_3 and SiO_2 nanoparticles and its nanofluids

Sol-gel procedure was engaged for the synthesis of Al_2O_3 and SiO_2 ceramic nanoparticles. In a typical production of Al_2O_3 nanoparticles, 10 g of aluminium nitrate was amalgamated with 104 ml of ethanol, 70 ml of water, and 10 ml of polyethylene glycol (PEG) under constant stirring in a magnetic stirrer for 30 min. Then 16 ml of ammonia suspension drizzled drop wise inside the above mixture and stirred over 3 h at 80 °C resulting in the formation of a white gel. The gel was kept at room temperature overnight for aging. The white precipitate was obtained after the centrifugation process and washed three times using water and ethanol solutions to eliminate the residuals and impurities. Finally, the particles were calcinated at 750 °C in a muffle furnace and then grinded with mortar and pestle. SiO_2 nanoparticles have been prepared with TEOS, water, ethanol, PEG also ammonia solution in the quantity of 20 ml, 35 ml, 100 ml, 35 ml, and 10 ml respectively under vigorous stirring using the magnetic stirrer. Finally, the obtained white slurry gel was dried and calcinated at 750 °C for 5 h in a muffle furnace. The synthesized salts of white agglomerates were powdered using mortar and pestle.

The production of hybrid nanofluids was carried out through the famous two step mode with synthesized Al_2O_3 and SiO_2 nanoparticles, which accounts for producing bulk nanofluids with low cost. In the first step of preparing Al_2O_3–SiO_2 hybrid nanofluid, the nanoparticles were taken in the ratio of 50:50 each by weight concentration of each type of nanoparticles and dispersed in 60% water and 40% ethylene glycol. To overcome the stability, 2 g of challenge CTAB surfactant is added to above combination [34, 36]. Subsequently, ultrasonic vibration using ultrasonicator (170V AC – 270 V AC, 50 Hz, operating frequency 50 kHz, single phase model, Labline make, Mumbai, Maharashtra) of 30 min for each sample is employed to break the clustering the solid particles and uniform scattering of the particles inside base fluids [28, 40]. Thus the hybrid Al_2O_3–SiO_2 nanofluids for several volume concentrations (ϕ) have been prepared at room temperature by the eq. (1)

$$\phi = \frac{w_{np}/\rho_{np}}{w_{np}/\rho_{np} + w_{bf}/\rho_{bf}} X\ 100 \tag{1}$$

where, w_{np}w$_{\mathrm{np}}$ is the weight of both nanoparticles, w_{bf} is the weight of W/EG solution,ρ_{np} is both nanoparticles density, and $\rho_{\mathrm{bf}}$is W/EG solution density.

Cylindrical heat pipe experimental setup

The schematic of cylindrical screen mesh heat pipe apparatus set up employed for examining the heat transfer performance is shown in Fig. 1. Heat pipe works on the phenomenon of phase change with capillary action. Initially, cylindrical copper tube and zinc wire screen mesh wick are cut into the desired size. Proper cleaning assembly procedures eliminate the formation of gas inside the heat pipe during construction. The cylindrical heat pipe is fabricated with copper material. It contains evaporator (300 mm), adiabatic (400 mm), and condenser (300 mm) sectors. The inner diameter has 10.9 mm diameter and outer has 12.7 mm diameter, and length is about 1000 mm. Its interior is surrounded with a metal (zinc) wire mesh. One end of heat pipe is blocked up with the metal lid and the other end is left open for charging nanofluids. The three K-type thermocouples (± 2% accuracy) are inserted on the surfaces of the heat pipe

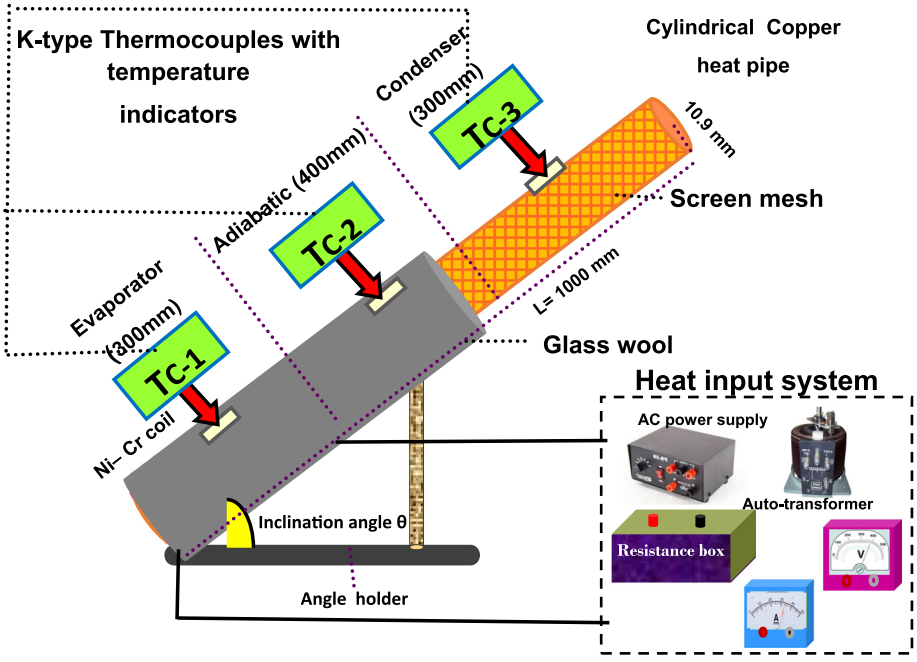

Fig. 1 Schematic of experimental heat pipe system

through small holes. There are three temperature indicators joined with three thermocouples. The input heating system consists of a Nichrome (Ni-Cr) heating coil associated with 230 V, 50 Hz AC power input, an autotransformer (0–230 V), an ammeter (0–1 A), and a voltmeter (0–150 V) for heating the evaporator section. This input heating system is attached with the heat pipe. Atmospheric air cools the condenser section. Glass wool of 20 mm thickness is used for minimizing the heat loss carefully which is wounded around the evaporator and adiabatic regions. The power applied to the heat pipe is estimated with the voltage and current provided with ± 0.5% accuracy.

Al_2O_3–SiO_2 hybrid nanofluids of six various volume concentrations (0%, 0.0125%, 0.025%, 0.05%, 0.075, and 0.1%) were used for experimental investigation. Initially, the experiment was performed with 0% volume concentration (base fluid alone), subsequently with Al_2O_3, SiO_2, and Al_2O_3–SiO_2 nanofluids volume concentrations. The orientation of heat pipe was maintained at three angles 30, 45, and 60°. The temperature in evaporator and condenser sections was measured for 30, 60, and 90 W input heat powers. Five set of values was recorded for each particles volume concentrations for the accuracy of the values. The values were noted every time after the system attained the stable position. As of the experimental outcomes, thermal resistance (R) and heat transfer coefficient (h) of cylindrical pipe were calculated.

Data reduction and uncertainty examination

From the experimentation data, thermal values R and h values are estimated through the following equations.

The thermal resistance is calculated by the eq. (2)

$$R = [T_e - T_c]/Q \tag{2}$$

The heat transfer coefficient (h) was calculated using eq. (3) from the literature [21, 39, 42] as follows.

$$h = \frac{Q}{A(T_e - T_c)} \tag{3}$$

where evaporator temperature is denoted as T_e and condenser temperature is represented as T_c at the stable position, Q denotes heat Power (Q = IxV), and A indicates the interior heat pipe area which is equal to πdl (d specifies heat pipe interior diameter (m) and l represents length (m)).

The uncertainties in heat pipe experimental data were evaluated by the standard method [42]. The uncertainty of any variable such as R_v, the uncertainty interval for independent experimental measured variables (x_i) can be calculated using the following eq. (4)

$$U_{R_i} = \frac{x_i}{R_v}\frac{\partial R_v}{\partial x_i}U_{x_i} \tag{4}$$

where U_{Ri} is the uncertainty in the result (i.e., the approximate possible error introduced in calculating one parameter) and R_v is a parameter calculated using computable quantities; U_{xi} is measurement error for the experimental measured variable and determined by dividing the measurement precision into the minimum measured value. The uncertainties of various measurements are calculated below

$$\text{The uncertainty invVoltage } (U_v) = \pm\frac{0.01}{49.5} = \pm 2.53 \times 10^{-4} \approx \pm 0.8\%$$

$$\text{The uncertainty in current } (U_c) = \pm\frac{0.01}{0.5} = \pm 0.02 \approx \pm 2\%$$

$$\text{The uncertainty in area } (U_A) = \pm\frac{0.02}{24} = \pm 8.3 \times 10^{-4} \approx \pm 0.8\%$$

The maximum uncertainty in R can be calculated for all values of x_i (i = 1, 2, 3. . . n) by the eq. (5)

$$U_{R_i} = \left[\left(\frac{x_1}{R_v}\frac{\partial R_v}{\partial x_1}U_{x_1}\right) + \left(\frac{x_2}{R_v}\frac{\partial R_v}{\partial x_2}U_{x_2}\right) + \ldots\ldots + \left(\frac{x_n}{R_v}\frac{\partial R_v}{\partial x_n}U_n\right)\right] \tag{5}$$

The maximum uncertainties in power (Q), R, and h data were computed as through the relations (6), (7), and (8). The values of uncertainties in Q, R, and h are found to be ± 2.76%, ± 2.76%, and ± 2.91% respectively that are optimum only.

$$\frac{\Delta Q}{Q} = \sqrt{\left(\frac{\Delta V}{V}\right)^2 + \left(\frac{\Delta V}{V}\right)^2} = \pm 2.76\% \tag{6}$$

$$\frac{\Delta R}{R} = \sqrt{\left(\frac{\Delta Q}{Q}\right)^2 + \left(\frac{\Delta\left(\Delta T_{e/c}\right)}{\Delta T_{e/c}}\right)^2} = \pm 2.76\% \tag{7}$$

$$\frac{\Delta h}{h} = \sqrt{\left(\frac{\Delta Q}{Q}\right)^2 + \left(\frac{\Delta A_{e/c}}{A_{e/c}}\right)^2 + \left(\frac{\Delta\left(\Delta T_{e/c}\right)}{\Delta T_{e/c}}\right)^2} = 2.91\% \tag{8}$$

Response surface methodology

One of the designs of experiment (DOE) methods used in engineering applications is response surface methodology (RSM). It is the technique used to identify the influences of the input parameters on considered responses in association with statistical and mathematical techniques [35]. The input parameters and execution scale are commonly referred to as independent variables and response respectively [29]. The attention of present work is of a regression model development of approximation using empirical data on thermal resistance and heat transfer coefficient to forecast response variables using RSM. The ability and dependability of the developed regression model have been examined through the analysis of variance (ANOVA) statistical technique. Sum of squares deals with the source of variance. The degrees of freedom represent total levels considered for experiment minus one. The ratio between sum of square values of every element and its respective degrees of freedom is considered as mean square. The ratio between the mean square of each factor and mean square of residual is called *F* ratio. ANOVA method was used to analyze the components such as coefficient of variation (R-square), Fisher's test (*F* test), and probabilities value (*P* value) which is essential variables for the prediction of appropriation of the models developed using regression analysis.

Results and discussion

In the first section, the structural and surface characterization (powder XRD, SEM, with EDS) of the prepared nanoparticles is presented. In the second section, the heat transfer performance of the hybrid nanofluids are explained with a comparison between hybrid and single Al_2O_3 and SiO_2 nanofluids. The third section analyzes the RSM approach with statistical techniques and validation.

Al_2O_3 and SiO_2 nanoparticles characterization studies

Powder X-ray diffraction method analysis

Figure 2a and b illustrates XRD pattern of aluminium oxide and silicon dioxide nanoparticles made through sol-gel manner. The phase and crystal arrangements of the Al_2O_3 as well as SiO_2 nanoparticles have been determined using X-ray diffractometer (X'pert-Pro). The 2θ testing has been directed from 10 to 80° at 0.05° range. Strong peaks spotted in Fig. 2a related to scattering angles 36.64°, 45.69°, 60.24°, and 66.07° denoting hkl on Miller indices (010), (121), (123), and (118) respectively. The miller indices planes corresponding to Bragg's peaks exhibit the orthorhombic structure of Al_2O_3 nanoparticles well matched with the JCPDS card no: 46-1215. Similarly, the diffraction peaks (Fig. 2b) intensify 22.22°, 44.6°, 65.42°, and 77.55° scattering angled that are associated with (101), (202), (204), and (401) miller indices planes respectively having the tetragonal structure of SiO_2 solid particles. The peak at 2θ = 22° indicates that SiO_2 particles were formed by small nanocrystals and the slight broadening of the peak is due to the effect of smaller grain size. The XRD pattern of SiO_2 particles is in good agreement with JCPDS card no: 76-0939. Examination of previous results denoted that the SiO_2 particles are amorphous in nature and size of the particle was above 50 nm [13, 15]. The increase in the crystalline nature of SiO_2 particles and smaller sized

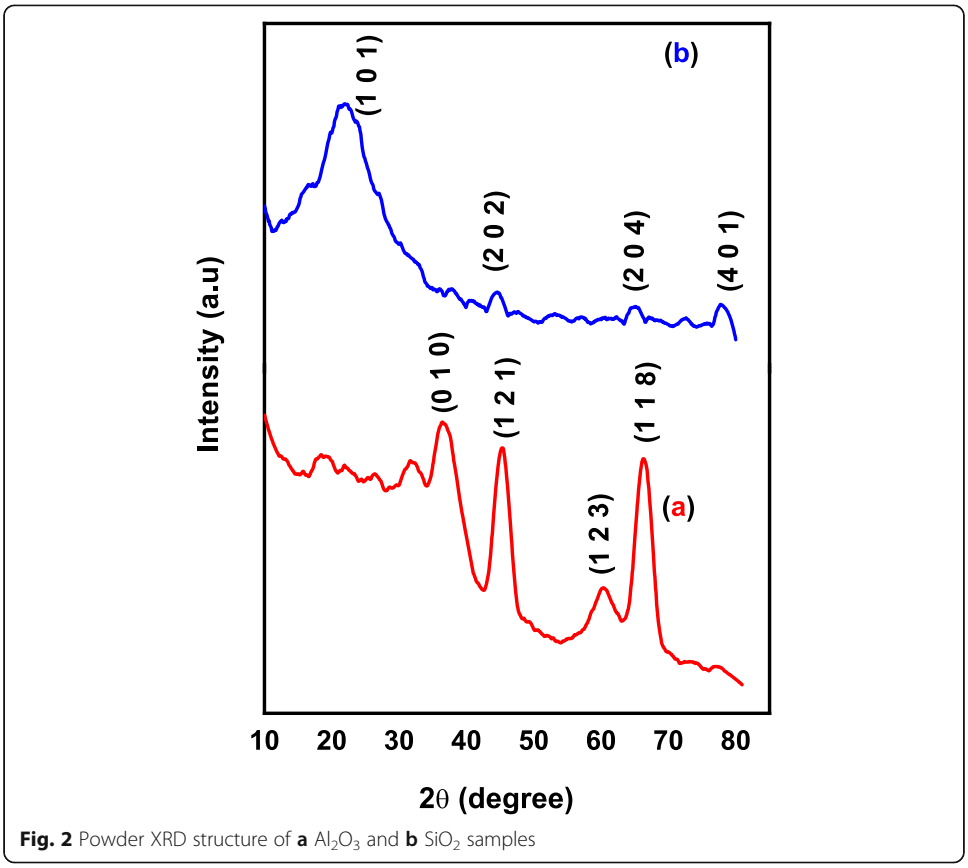

Fig. 2 Powder XRD structure of **a** Al_2O_3 and **b** SiO_2 samples

nanoparticles were due to the addition of polymer surfactant PEG. The mean crystallites size (D) is assessed by means of Debye–Scherrer Eq. (9)

$$D = K\lambda/\beta \cos\theta \tag{9}$$

where K indicates constant shape factor (1.9), λ denotes incident X-ray's wavelength (1.5405 Å), and β specifies full width at half maximum as well as θ stands for scattering angle. As of obtained XRD values, the mean crystallite size of Al_2O_3 and SiO_2 particles were found about 6 nm and 25 nm respectively. Smaller size nanoparticles exhibit a better performance in thermal conductivity and heat transfer properties [30].

Scanning electron microscope analysis

Scanning electron microscope analysis of nanoparticles is used for the representation of the surface structure of the samples through high-resolution images. JEOL, JSM 6390 device recorded the scanning electron microscope (SEM) pictures of Al_2O_3 and SiO_2 nanoparticles. It is revealed from the SEM results of Al_2O_3 nanoparticles with the histogram in Fig. 3 that the Al_2O_3 nanoparticles are mostly in a spherical shape with slight clusters of the particles. These results are in best agreement with those reported works [10, 25]. Besides, the size distribution of Al_2O_3 nanoparticles has been displayed through a histogram graph. It could be observed that the nanoparticles are distributed in the diameter range of 25–125 nm and most of the nanoparticles fall around 60 nm diameter. The Gaussian fit over the distribution denotes nano Al_2O_3 particles mean

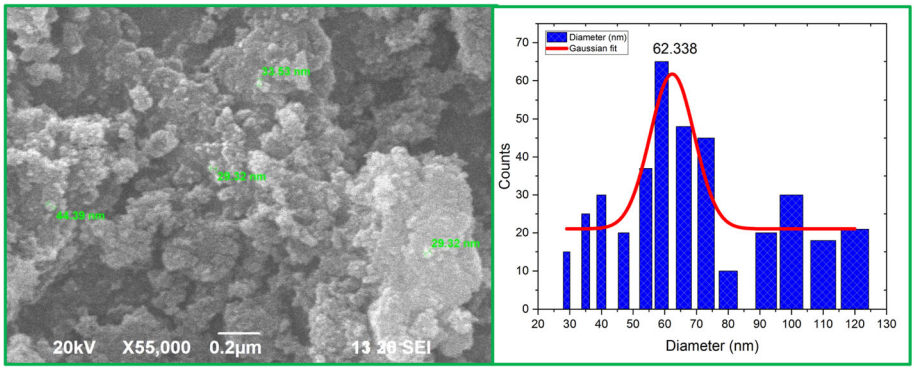

Fig. 3 SEM with histogram pattern of Al_2O_3 nanoparticles

size is 62.338 nm. Reduced dimension of the as-synthesized aluminium oxide nanoparticles is due to the addition of the polymer surfactant polyethylene glycol.

The SEM images of SiO_2 nanoparticles with histogram in Fig. 4 indicate that the spherical-shaped SiO_2 nanoparticles have a small aggregation with the neighboring nanoparticles. The aggregation of the SiO_2 nanoparticles is obtained due to the existence of a weak covalent bond between the atoms. From the histogram chart, it is confirmed that the SiO_2 nanoparticles having the size around 61 nm since most of the particles lie with this diameter range. The size distribution of SiO_2 particles is ranging from 40 to 100 nm. The obtained morphology of SiO_2 nanoparticles shows better results than the previous reports [13, 15] due to the addition of surfactant PEG. Controlling in size of both nanoparticles was accomplished as a consequence of balanced nucleation growth of nanoparticles. In addition, the size and morphology could be preciously tuned in nanometric scale by controlling the saturation rate during the second stage with optimum concentration.

Heat transfer performance analysis of heat pipe

Thermal ability in heat pipe is not only influenced by working fluid concentration but also heat pipe orientation, heat input power, and gravity effect. Therefore, it is necessary to analyze the thermal performance based on the above mentioned factors.

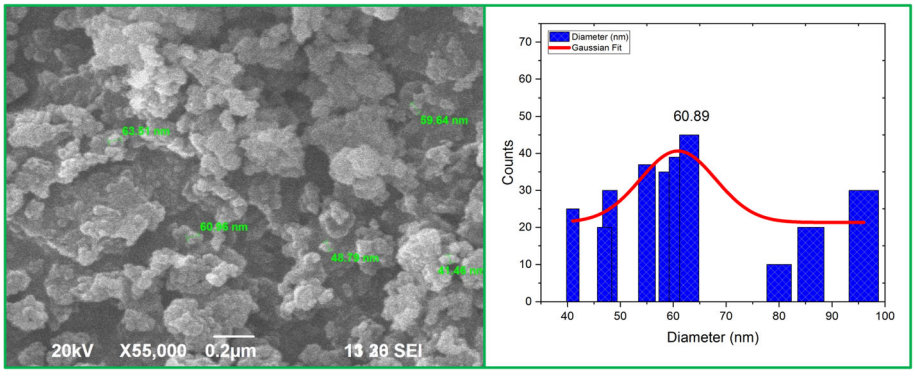

Fig. 4 SEM with histogram pattern of SiO_2 nanoparticles

Effect of heat pipe orientation upon thermal resistivity

Thermal resistance determined from Al_2O_3–SiO_2 nanofluids in cylindrical heat pipe experimentation for at various inclined angles (30, 45, and 60°) are drawn in Fig. 5a–c. The thermal resistivity decreases from 30° to 45° orientation of heat pipe and also increased after 45° to 60° angle for all the heat input powers in the range 30, 60, and 90 W. This is due to the high influence of gravitational force action between the condenser and evaporator regions. Usually, the vapor movement within the heat pipe is owing to the change in density of fluids. The mutual action of gravity and the force in the wick structure initiates the returning of condensed vapor back to the evaporator area. Beyond the inclined angle 45°, the heat provided at the evaporator region is insufficient. Hence, heat transfer action is decreased radially and also leads to increased thermal resistance. Also, below the inclination angle 30°, the heat transfer characteristics seem to be decreased. The researchers have also reported that this range of inclination angle of heat pipe yielded the better heat transfer performance than horizontal (0°) and vertical positions (90°) [13, 27]. Hence, the orientation of heat pipe was maintained in the angle ranging from 30° to 60° angle.

Effect of power and volume concentrations on thermal resistivity

Figure 6 was drawn between the volume concentration of nanofluids and thermal resistance for three different power inputs (30, 60, and 90 W). According to the graph, it is clear that nanoparticles addition with base solution diminishes the values of thermal

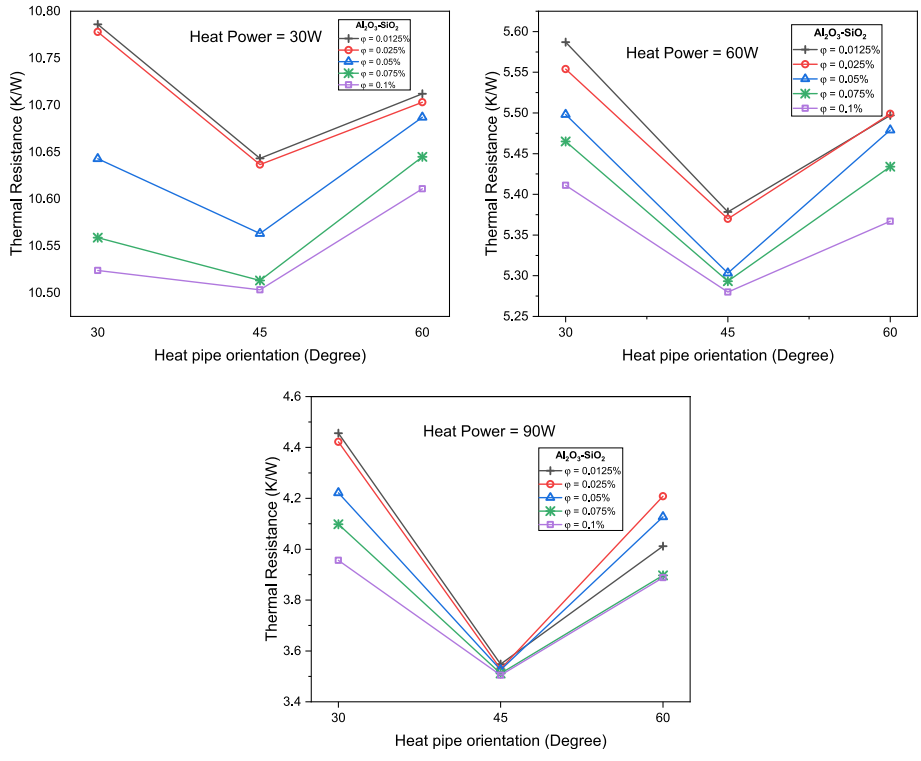

Fig. 5 The effect of heat pipe orientation on thermal resistance at **a** 30 W, **b** 60 W, and **c** 90 W heat input power

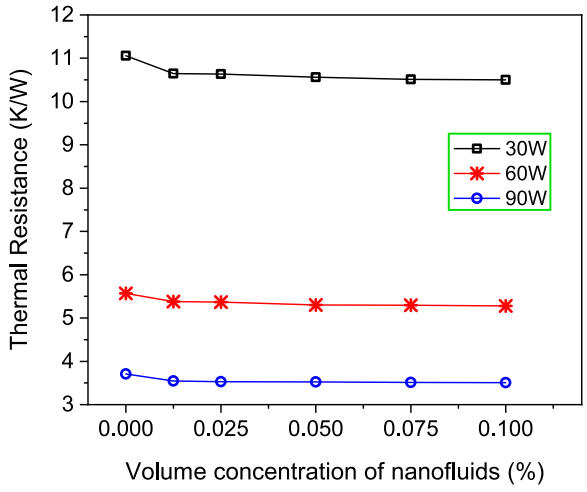

Fig. 6 Effect of volume concentration and heat power input on thermal resistance

resistance dramatically. As of increase in surface wettability, resistivity of hybrid nanofluids seems to be decreased. This is caused by Al_2O_3–SiO_2 nanoparticles settlement of above wick structures while heating takes place in evaporation zone. Moreover, thermal resistance shows a decreasing phenomenon with increasing heat power inputs. At high heat input, the formation of a fluid layer upon wick structure due to the base fluid is eliminated [13]. The maximum value of thermal resistance 3.5 K/W is noticed at 90 W heat input for 0.1% volume concentration of hybrid Al_2O_3–SiO_2 nanofluid. This seems to be 5.54% higher than W/EG fluid. This decrement in thermal resistance at a higher concentration of nanofluids exhibits the improved efficiency of nanofluids in the heat pipe.

Comparison on thermal resistance of single and hybrid nanofluids

Figure 7 displays thermal resistance decrement comparison between single component (Al_2O_3 and SiO_2) and hybrid nanofluids (Al_2O_3–SiO_2) for three heat power inputs at maximum concentration 0.1%. The comparative analysis of the single and hybrid nanofluids maintained at the optimum orientation of heat pipe at 45°. The decrement percentage can be assessed through the ratio of thermal resistance variation between nanofluids and base fluid. High percentage in decrement indicates the lower value of thermal resistance and vice versa. In the figure, it is confirmed the thermal resistance decrement percentage for Al_2O_3–SiO_2 hybrid nanofluids is maximum, denoting the lower value of thermal resistance than the Al_2O_3 and SiO_2 single nanofluids. It shows maximum 5.54% reduction at 90 W for 0.1% volume concentration than the base fluid while single nanofluids exhibited lower percentage decrement in all power inputs.

Heat transfer coefficient

Figure 8 was plotted between volume concentrations and heat transfer coefficient values with 45° inclination angle. The incorporation of 0.1% nanoparticles in 90 W power indicates the maximum heat transfer coefficient is 62.01 W/m^2K, which is 43.16% more than W/EG fluid mixture. Higher heat transfer values in this hybrid fluid are achieved by low thermal resistance over liquid layer. The minimum and maximum

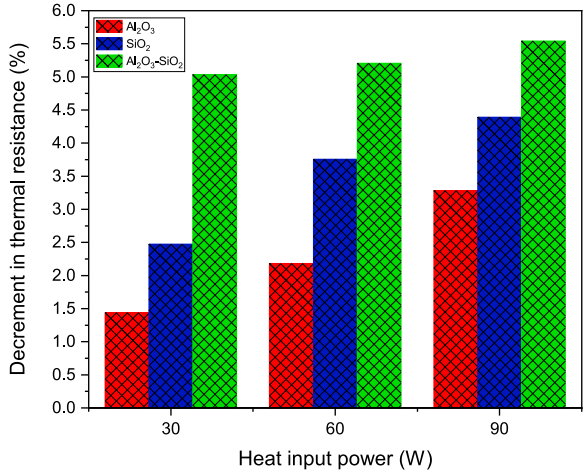

Fig. 7 Comparison on thermal resistance of single and hybrid nanofluids for 0.1% volume concentration at 45° orientation of heat pipe

heat transfer coefficient value of 14.88 W/m^2 K and 62.01 W/m^2 K was observed at low and higher volume concentrations (0.0125% and 0.1%) with low and high powers of 30 and 90 W respectively.

Heat transfer coefficient increases by 43.16% at 0.1% fraction on hybrid Al_2O_3–SiO_2 fluids with respect to base solution at 90 W. When temperature increases, thermal conductivity values in nanofluids tremendously increases and viscosity decreases according to base fluid particularly at higher particle concentrations. The augmented heat transfer coefficient value with hybrid Al_2O_3–SiO_2 nanofluids is superior to other nanofluids [13, 14, 43–45]. The comparison of heat transfer performance for various hybrid nanofluids with this hybrid Al_2O_3–SiO_2 nanofluids represented in Table 1 confirms the proficiency of hybrid Al_2O_3-SiO_2 nanofluids in cylindrical mesh heat pipe than other conventional fluids especially W/EG solution.

Figure 9 presents heat transfer coefficient increment comparison between single component (Al_2O_3 and SiO_2) and hybrid nanofluids (Al_2O_3–SiO_2) for at three heat power

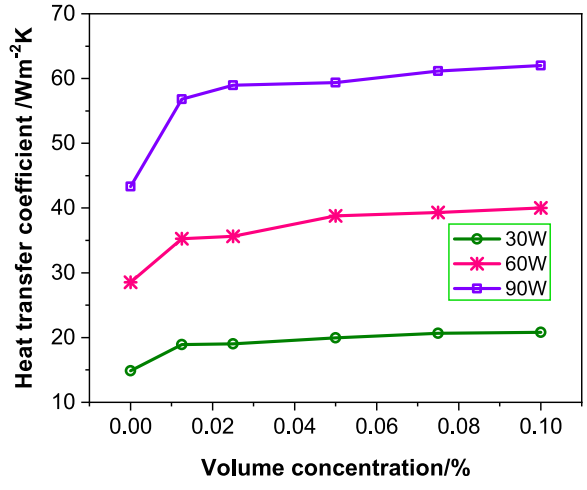

Fig. 8 Heat transfer coefficient of Al_2O_3–SiO_2 nanofluids as a function of heat input and volume concentrations

Table 1 Comparison in heat transfer performance of screen mesh type wick structure cylindrical heat pipe using nanofluids with present work

Nanofluid	Volume concentration	Operating parameters	Outcome	Literature
CuO/DI water	0.5, 1.0, 1.5%	Orientation (°): 0–90 Heat Load (W): 40–120	Evaporation and condensation Heat transfer coefficient were improved by 30.50% and 23.54% Respectively	Venkatachalapathy et al. [13]
Graphene oxide (GO)/ water	0.01%	Heat load (W): 25–450	Heat transfer coefficient was improved by 25.5%	Kim and Bang [14]
CuO/water	0.5, 1.0, 2.0%	Orientation (°): 30, 45, 60, and 90 Heat load (W): 0–180	Evaporator and condenser Heat transfer coefficient were improved by 22% and 5%	Wang et al. [43]
Cu/DI water		Heat Load (W): 100, 150, and 200	Heat transfer coefficient was enhanced by 40%	Solomon et al. [44]
CuO, Al_2O_3/ DI water	0.5, 1.0, 1.5%	Orientation (Deg): 0, 30,45, 60, 75, 90 Heat load (W): 10–160	Heat transfer coefficient was increased by 32.99% and 24.59% for CuO and Al_2O_3 respectively	Vijaykumar et al. [45]
Al_2O_3-SiO_2/ W-EG	0.0125, 0.025, 0.05, 0.075, 0.01%	Orientation (°): 30,45, and 60 Heat Load (W): 30, 60, and 90	Heat transfer coefficient was increased by 43.16%	Present study

inputs at maximum concentration 0.1%. The comparative analysis displayed the results of the single and hybrid nanofluids at the optimum orientation of heat pipe maintained at 45°. The increment percentage can be calculated by the ratio of difference in heat transfer coefficient between nanofluids and base fluid. High percentage in increment indicates the higher heat transfer ability. From graph, it is established that heat transfer coefficient increment percentage for Al_2O_3–SiO_2 hybrid nanofluids is maximum, denoting the augmented heat transfer performance than the Al_2O_3 and SiO_2 single nanofluids. It shows maximum 43.16% augmentation at 90 W for 0.1% volume concentration than the base fluid whereas single nanofluids exhibited lower increment percentage for all heat power inputs.

RSM approach with statistical technique

The empirical data collected from experimental setup are given as input to the response surface methodology. Design-Expert software is adopted to analyze the experimental data. The user-defined data format is used for statistical analysis.

ANOVA is a standard statistical tool employed to estimate the variance size between experimental data set. Table 2 represents the model summary of thermal resistance and heat transfer coefficient with RSM statistical analysis. This Table 2 values depict that the quadratic formula is best to predict the thermal resistance and heat transfer coefficient value. The achievement of good matching between the predicted and developed models with the correlation is possible only if the value of R-squared is near to 1 [40]. The four different models named linear, 2factorial interaction (2FI), quadratic, and cubic were developed based on regression analysis. It is suggested the quadratic model

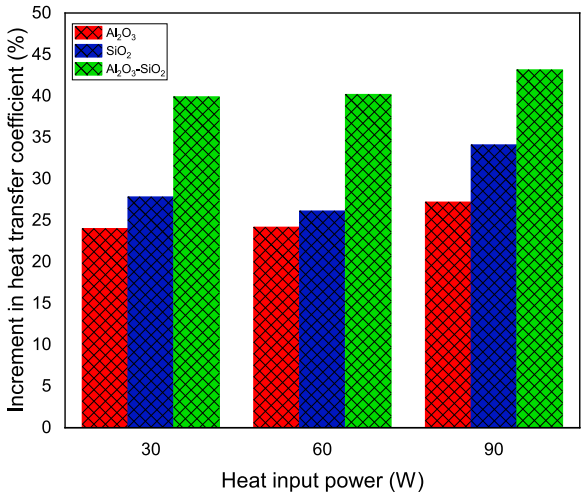

Fig. 9 Comparison on heat transfer coefficient of single and hybrid nanofluids for 0.1% volume concentration at 45° orientation of heat pipe

provides the best correlation with the experimental data since R^2 is near to 1in both thermal resistance and heat transfer coefficient results. Also, the "Predicted R^2" of 0.9988 and 0.9556 are near to the "Adjusted R^2" values of 0.9994 and 0.9761 for thermal resistance as well as heat transfer coefficient respectively. This shows the accuracy of both the developed models in this work. The signal to noise ratio is measured by "Adequate Precision" value. The adequate precision value larger than 4 is desirable for navigating the design space [46]. The adequate precision values of 167.941 and 32.201 for thermal resistance and heat transfer coefficient indicate that the models can be used for navigating the design space. Both the thermal resistance and heat transfer coefficient response values obtained in this work is very adjacent to each other denoting the accuracy of thr developed RSM models to predict the thermal resistance and heat transfer coefficient data with the cylindrical mesh type heat pipe. Generally, RSM proposes a proficiency to be used in the thermal engineering field exclusively in nanofluids that are engaged for heat and mass transfer applications in solar collectors, heat exchangers [37–40].

Table 2 Model summary of responses

Model	SD	R squared	Adjusted R squared	Predicted R squared	Adequate precision	
Thermal resistance						
Linear	0.90	0.9252	0.9152	0.8970	19.963	
2FI	0.93	0.9254	0.9094	0.8806	16.683	
Quadratic	0.077	0.9996	0.9994	0.9988	167.941	Suggested
Cubic	0.058	0.9998	0.9996	0.9990	181.363	Aliased
Heat transfer coefficient						
Linear	3.45	0.9618	0.9567	0.9406	33.402	
2FI	3.27	0.9679	0.9610	0.9393	30.856	
Quadratic	2.56	0.9831	0.9761	0.9556	32.201	Suggested
Cubic	1.97	0.9925	0.9859	0.9570	33.864	Aliased

The significant model terms are recognized by using the ANOVA table. Table 3 shows the ANOVA test results of thermal resistance and heat transfer coefficient response surface quadratic model for hybrid Al_2O_3–SiO_2 nanofluids. From Table 3, the *F* value of the model for thermal resistance and heat transfer coefficient is found to be 5572.90 and 139.72 which implies that both the regression models are significant. The probability values (Prob values) are used to examine the importance of each term. The model terms are said to important if the "Prob > *F*" lies below 0.05 and "Prob > *F*" lies above 0.1000 implies the unimportance of model terms. In this connection, the two models developed in this works showed the statistic significance of volume concentration and heat power both model terms.

Response surface plot analysis

Figures 10 and 11 show the interaction plots for thermal resistance and heat transfer coefficient. The thermal resistance interaction plot and response plot in Fig. 10a, b represents that the high level of volume concentration with high heat input power gives the minimum thermal resistance. Heat transfer coefficient interaction plot and response plot in Fig. 11a, b illustrate that a high level of volume concentration with a high level of power produces maximum heat transfer coefficient.

Table 3 Analysis of variance of all responses

Source	Sum of squares	Degrees of freedom	Mean square	F value	*P*-value Prob > F	
Thermal resistance ANOVA table						
Model	163.53	5	32.71	5572.90	< 0.0001	Significant
A-Volume Concentration	*0.15*	*1*	*0.15*	*25.04*	*0.0003*	
B-Power	*145.88*	*1*	*145.88*	*24856.99*	*< 0.0001*	
AB	*0.028*	*1*	*0.028*	*4.74*	*0.0502*	
A^2	*0.058*	*1*	*0.058*	*9.90*	*0.0084*	
B^2	*12.08*	*1*	*12.08*	*2058.05*	*< 0.0001*	
Residual	0.070	12	5.869E-003			
Cor total	163.60	17				
Heat transfer coefficient ANOVA table						
Model	4592.78	5	918.56	139.72	< 0.0001	significant
A-Volume Concentration	*181.81*	*1*	*181.81*	*27.65*	*0.0002*	
B-Power	*4296.22*	*1*	*4296.22*	*653.49*	*< 0.0001*	
AB	*28.66*	*1*	*28.66*	*4.36*	*0.0588*	
A^2	*59.07*	*1*	*59.07*	*8.98*	*0.0111*	
B^2	*11.96*	*1*	*11.96*	*1.82*	*0.2023*	
Residual	78.89	12	6.57			
Cor total	4671.67	17				

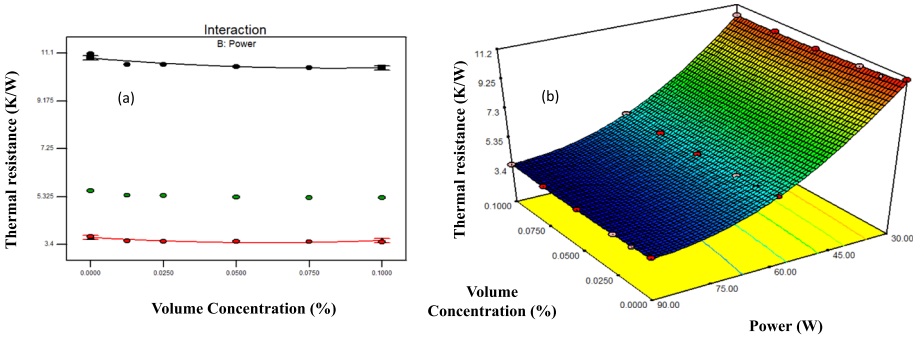

Fig. 10 a Interaction effect of thermal resistance of hybrid nanofluid. **b** Response surface plot

Regression analysis

The relationship between input factors and response needs a declaration of the statistical model. Concerning Figs. 10a and 11a, the interaction plots of thermal resistance and heat transfer coefficient does not follow the straight line. Hence, these models incorporated the polynomial regression models. Equations 10 and 11 represent the quadratic formulae for thermal resistance (R) and heat transfer coefficient (h).

$$R = 19.72167 - 11.24794 * \phi - 0.35201 * P + 0.04563 * \phi P + 59.40435 * \phi^2 + 1.93076E - 003 * P^2 \quad (10)$$

$$h = 2.86346 + 191.95901 * \phi + 0.3368 * P + 1.46458 * \phi P - 1894.44815 * \phi^2 + 1.92138E - 003 * P^2 \quad (11)$$

Validation of RSM models

Figure 12a, b shows the validation of RSM models with experimental results for thermal resistance and heat transfer coefficient. The average deviation between experimental results and RSM models are – 2.36% and – 12.74% for thermal resistance and heat transfer coefficient respectively. The maximum deviations are observed as – 5.15% and – 33.46% for 0.1% volume concentration at 60 W heat input power. Table 4 displays the percentage of deviation between the experimental and RSM model results. The difference between the predicted values and experimental value has a minor deviation that implies the high accuracy in the modeling approach. Thus, eqs. 8 and 9 can be used to predict the thermal resistance and heat transfer coefficient values of heat pipe with Al_2O_3–SiO_2 hybrid nanofluids within the range of input parameters considered in this experiment.

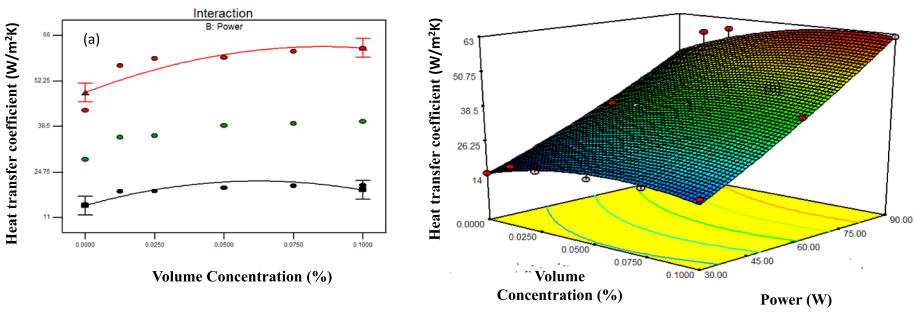

Fig. 11 a Interaction effect of heat transfer coefficient for hybrid nanofluid. **b** Response surface plot

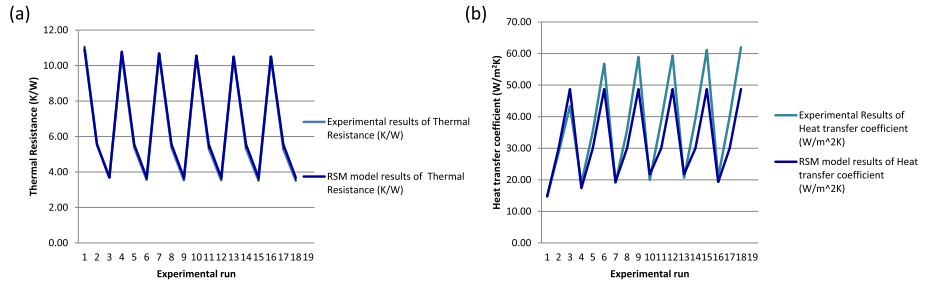

Fig. 12 Validation of RSM results with experimental data of **a** thermal resistance and **b** heat transfer coefficient

Conclusions

This work deals with the enhancement of heat transfer characteristics of cylindrical screen mesh heat pipe using hybrid Al_2O_3 and SiO_2 nanoparticles with W/EG binary mixture. The experimental results showed that the heat transfer capacity increases with volume concentrations of hybrid nanofluids and heat input power. The following main conclusions were obtained from the present study:

Table 4 Comparison between experimental and RSM model results

Volume concentration (%)	Power (W)	Experimental results using heat pipe		RSM model results		% of Deviation	
		Thermal resistance (K/W)	Heat transfer coefficient (W/m^2 K)	Thermal resistance (K/W)	Heat transfer coefficient (W/m^2 K)	Thermal resistance (K/W)	Heat transfer coefficient (W/m^2 K)
0	30	11.06	14.88	10.90	14.70	1.48	− 1.26
	60	5.57	28.55	5.55	29.99	0.39	4.79
	90	3.71	43.32	3.68	48.74	0.75	11.12
0.0125	30	10.64	18.93	10.78	17.35	− 1.33	− 9.12
	60	5.38	35.27	5.55	29.99	− 3.23	− 17.62
	90	3.55	56.79	3.68	48.74	− 3.72	− 16.53
0.025	30	10.64	19.01	10.69	19.41	− 0.49	2.04
	60	5.37	35.63	5.55	29.99	− 3.39	− 18.82
	90	3.53	58.96	3.68	48.74	− 4.28	− 20.97
0.05	30	10.56	19.97	10.55	21.76	0.09	8.22
	60	5.30	38.78	5.55	29.99	− 4.69	− 29.33
	90	3.53	59.36	3.68	48.74	− 4.38	− 21.79
0.075	30	10.51	20.67	10.49	21.73	0.20	4.88
	60	5.29	39.31	5.55	29.99	− 4.88	− 31.07
	90	3.51	61.15	3.68	48.74	− 4.81	− 25.47
0.1	30	10.50	20.82	10.51	19.34	− 0.02	− 7.64
	60	5.28	40.02	5.55	29.99	− 5.15	− 33.46
	90	3.50	62.02	3.68	48.74	− 5.01	− 27.25
					Mean:	**− 2.36%**	**− 12.74%**

- Al_2O_3 and SiO_2 nanoparticles were synthesized using the sol-gel method. XRD analysis revealed the orthorhombic and tetragonal structures of nanoparticles with the average crystallite sizes of 6 and 25 nm respectively. From SEM analysis, the observed structures for both Al_2O_3 and SiO_2 nanoparticles were spherical and the particles size falls around 62 nm and 61 nm respectively.
- The thermal resistance of the heat pipe with Al_2O_3–SiO_2 hybrid nanofluids is reduced by 5.54% and heat transfer coefficient is enhanced by 43.16% than base fluid W/EG base fluid mixture at higher volume concentration (0.1%) and high power (90W).
- The superior enhancement in heat transfer characteristics of heat pipe suggested this novel hybrid Al_2O_3–SiO_2 nanofluid could be a substitute for heat transfer applications in various devices.
- The parameter influence and empirical models were established based on statistical techniques response surface methodology and regression analyses. Based on the ANOVA table, the influencing independent parameters on thermal resistance and heat transfer coefficient are volume concentration as well as power, which are considered as the significant input parameters. Both the thermal resistance and heat transfer coefficient response values obtained are very near to each other denoting the accuracy of the developed RSM models.
- Validation of results implied that the developed quadratic models are able to predict well the thermal resistance and heat transfer coefficient of cylindrical heat pipe with average percentage of deviation (– 2.36% and – 12.74%) less than 1% against the experimental results for the heat power range 30–90 W at the inclined angle 45° in the volume concentration ranging from 0.0125 to 0.1%. Hence, it is emphasized that these proposed mathematical models can be utilized for prediction of heat transfer coefficient and thermal resistivity of Al_2O_3–SiO_2 hybrid nanofluids with cylindrical screen mesh heat pipe.

Abbreviations

Al_2O_3: Aluminium oxide; SiO_2: Silicon dioxide; CuO: Copper oxide; Fe_2O_3: Ferrous oxide; TiO_2: Titanium oxide; ZnO: Zinc oxide; TEOS: Tetra ethyl ortho silicate; PEG: Polyethylene glycol; CTAB: Cationic surfactant; W: Water; EG: Ethylene glycol; eq.: Equation; eqs.: Equations; Ni-Cr: Nichrome; Al: Aluminium; O: Oxygen; Si: Silicon; DOE: Design of experiment; RSM: Response surface methodology; ANOVA: Analysis of variance; *F* test: Fisher's test; prob: Probability; ANN: Artificial Neural Network; w_{np}: Weight of both nanoparticles; w_{bf}: Weight of W/EG solution; ρ_{np}: Nanoparticles density; ρ_{bf}: W/EG solution density; *R*: Thermal resistance; *h*: Heat transfer coefficient; T_e: Evaporator temperature; T_c: Condenser temperature; *Q*: Heat power; *P*: Power; *A*: Interior heat pipe area; *d*: Heat pipe interior diameter; *l*: Heat pipe length; XRD: X-ray diffraction; SEM: Scanning electron microscope; EDS: Energy dispersive X-ray diffraction; *D*: Mean crystallites size; *K*: Constant shape factor; λ: Incident X-ray's wavelength; β: Full width at half maximum; θ: Scattering angle; U_{Ri}: The uncertainty in the result; R_v: Parameter calculated using computable quantities; U_{xi}: Measurement error for the experimental measured variable; U_v: The uncertainty in voltage; U_c: The uncertainty in current; U_A: The uncertainty in area

Acknowledgements

Not applicable.

Authors' contributions

All authors contributed to the study conception and design. RV investigated the experimental data and prepared the original draft. TB reviewed, edited and validated the results and manuscript. BS Conceptualized and analyzed the results. All authors have read and approved the manuscript.

Funding

No funds, grants, or other support was received.

Availability of data and materials

The datasets generated during and/or analyzed during the current study are available from the corresponding author on reasonable request.

Declarations

Competing interests
The authors declare no competing interests.

Author details
[1]PG & Research Department of Physics, Bishop Heber College (Affiliated to Bharathidasan University), Tiruchirappalli, Tamilnadu 620017, India. [2]Crystal Growth Laboratory, PG and Research Department of Physics, Periyar E.V.R College (Affiliated to Bharathidasan University), Tiruchirappalli, Tamilnadu 620023, India. [3]K. Ramakrishnan College of Technology (Affiliated to Anna University), Samayapuram, Tiruchirappalli, Tamilnadu 621112, India.

Received: 28 July 2021 Accepted: 8 October 2021
Published online: 21 November 2021

References
1. Yıldız C, Arıcı M, Karabay H (2019) Comparison of a theoretical and experimental thermal conductivity model on the heat transfer performance of Al_2O_3-SiO_2/water hybrid-nanofluid. Int J Heat Mass Transf 140:598–605. https://doi.org/10.1016/j.ijheatmasstransfer.2019.06.028
2. Lee HS (2011) Thermal Design, Heat Sinks, Thermo electrics heat pipes, compact heat exchangers and solar cells. Wiley, Newyork. https://doi.org/10.1002/9780470949979
3. Rahimi-Gorji M, Pourmehran O, Hatami M, Ganji DD (2015) Statistical optimization of microchannel heat sink (MCHS) geometry cooled by different nanofluids using RSM analysis. Eur Phys J Plus 130(2):22. https://doi.org/10.1140/epjp/i2015-15022-8
4. Żyła G (2016) Thermophysical properties of ethylene glycol based yttrium aluminum garnet ($Y_3Al_5O_{12}$–EG) nanofluids. Int J Heat Mass Transf 92:751–756. https://doi.org/10.1016/j.ijheatmasstransfer.2015.09.045
5. Che Sidik NA, Mahmud Jamil M, Aziz Japar WMA, Muhammad Adamu I (2017) A review on preparation methods, stability and applications of hybrid nanofluids. Renew Sust Energ Rev 80:1112–1122. https://doi.org/10.1016/j.rser.2017.05.221
6. Dhinesh Kumar D, Valan Arasu A (2018) A comprehensive review of preparation, characterization, properties and stability of hybrid nanofluids. Renew Sust Energ Rev 81:1669–1689. https://doi.org/10.1016/j.rser.2017.05.257
7. Mehrali M, Sadeghinezhad E, Rosen MA, Akhiani AR, Tahan Latibari S, Metselaar HSC (2015) Heat transfer and entropy generation for laminar forced convection flow of graphene nanoplatelets nanofluids in a horizontal tube. Int Commun Heat Mass Transf 66:23–31. https://doi.org/10.1016/j.icheatmasstransfer.2015.05.007
8. Zyła G, Cholewa M, Witek A (2012) Dependence of viscosity of suspensions of ceramic nanopowders in ethyl alcohol on concentration and temperature. Nanoscale Res Lett 7(1):412. https://doi.org/10.1186/1556-276X-7-412
9. Choi SUS (1995) Enhancing thermal conductivity of fluids with nanoparticles developments and applications of non-Newtonian flows. In: Siginer DA, Wang HP (eds) FED-Vol. 231/MD, vol 66. ASME, New York, pp 99–103
10. Chien H-T, Tsai C-I, Chen P-H, Chen P-Y (2003) Improvement on thermal performance of a disk-shaped miniature heat pipe with nanofluid, Fifth International Conference on Electronic Packaging Technology. Proceedings - Shanghai, China. Fifth International Conference on Electronic Packaging Technology Proceedings, pp 389–391
11. Alijani H, Çetin B, Akkus Y, Dursunkaya Z (2018) Effect of design and operating parameters on the thermal performance of aluminum flat grooved heat pipes. Appl Therm Eng 132:174–187. https://doi.org/10.1016/j.applthermaleng.2017.12.085
12. Poplaski LM, Benn SP, Faghr A (2017) Thermal performance of heat pipes using nanofluids. Int J Heat Mass Transf 107:358–371. https://doi.org/10.1016/j.ijheatmasstransfer.2016.10.111
13. Venkatachalapathy S, Kumaresan G, Suresh S (2015) Performance analysis of cylindrical heat pipe using nanofluids – an experimental study. Int J Multiphase Flow 72:188–197. https://doi.org/10.1016/j.ijmultiphaseflow.2015.02.006
14. Kim KM, Bang IC (2016) Effects of graphene oxide nanofluids on heat pipe performance and capillary limits. Int J Therm Sci 100:346–356. https://doi.org/10.1016/j.ijthermalsci.2015.10.015
15. Wan Z, Deng J, Li B, Xu Y, Wang X, Tang Y (2015) Thermal performance of a miniature loop heat pipe using water-copper nanofluid. Appl Therm Eng 78:712–719. https://doi.org/10.1016/j.applthermaleng.2014.11.010
16. Solomon AB, Ramachandran K, Asirvatham LG, Pillai BC (2014) Numerical analysis of a screen mesh wick heat pipe with Cu/water nanofluid. Int J Heat Mass Transf 75:523–533. https://doi.org/10.1016/j.ijheatmasstransfer.2014.04.007
17. Akbari A, Saidi MH (2018) Experimental investigation of nanofluid stability on thermal performance and flow regimes in pulsating heat pipe. J Therm Anal Calorim 135(3):1835–1847. https://doi.org/10.1007/s10973-018-7388-3
18. Salehi H, Zeinali Heris S, Koolivand Salooki M, Noei SH (2011) Designing a neural network for closed thermosyphon with nanofluid using a genetic algorithm. Braz J Chem Eng 28(1):157–168. https://doi.org/10.1590/S0104-66322011000100017
19. Ghanbarpour M, Nikkam N, Khodabandeh R, Toprak MS (2015) Improvement of heat transfer characteristics of cylindrical heat pipe by using SiC nanofluids. Appl Therm Eng 90:127–135. https://doi.org/10.1016/j.applthermaleng.2015.07.004
20. Heris SZ, Fallahi M, Shanbedi M, Amiri A (2016) Heat transfer performance of two-phase closed thermosyphon with oxidized CNT/water nanofluids. Heat Mass Transf 52(1):85–93. https://doi.org/10.1007/s00231-015-1548-9
21. Zeinali Heris S, Shokrgozar M, Poorpharhang S, Shanbedi M, Noie SH (2014) Experimental study of heat transfer of a car radiator with CuO/ethylene glycol-water as a coolant. J Dispers Sci Technol 35(5):677–684. https://doi.org/10.1080/01932691.2013.805301
22. Ilyas SU, Narahari M, Theng JTY, Pendyala (2019) Experimental evaluation of dispersion behavior, rheology and thermal analysis of functionalized zinc oxide-paraffin oil nanofluids. J Mol Liq 294:111613. https://doi.org/10.1016/j.molliq.2019.111613
23. Ranga Babu JA, Kumar KK, Srinivasa Rao S (2017) State-of-art review on hybrid nanofluids. Renew Sust Energ Rev 77:551–565. https://doi.org/10.1016/j.rser.2017.04.040
24. Esfe MH, Arani AAA, Rezaie M, Yan WM, Karimipour A (2015) Experimental determination of thermal conductivity and dynamic viscosity of Ag–MgO/water hybrid nanofluid. Int Commun Heat Mass Transf 66:189–195. https://doi.org/10.1016/j.icheatmasstransfer.2015.06.003
25. Nabil MF, Azmi WH, Abdul Hamid K, Mamat R, Hagos FY (2017) An experimental study on the thermal conductivity and dynamic viscosity of TiO_2-SiO_2 nanofluids in water: ethylene glycol mixture. Int Commun Heat Mass Transf 86:181–189. https://doi.org/10.1016/j.icheatmasstransfer.2017.05.024

26. Paul G, Philip J, Raj B, Das PK, Manna I (2011) Synthesis, characterization, and thermal property measurement of nano-$Al_{95}Zn_{05}$ dispersed nanofluid prepared by a two-step process. Int J Heat Mass Transf 54(15-16):3783–3788. https://doi.org/10.1016/j.ijheatmasstransfer.2011.02.044
27. Wang P-Y, Chen X-J, Liu Z-H, Liu Y-P (2012) Application of nanofluid in an inclined mesh wicked heat pipes. Thermochim Acta 339:100–108. https://doi.org/10.1016/j.tca.2012.04.011
28. Akilu S, Baheta AT, Said MAM, Minea AA, Sharma KV (2018) Properties of glycerol and ethylene glycol mixture based SiO_2-CuO_2/C hybrid nanofluid for enhanced solar energy transport. Solar Energy Mat and Solar Cells 179:118–128. https://doi.org/10.1016/j.solmat.2017.10.027
29. Esfe MH, Wongwises S, Naderi A, Asadi V, Safaei MR, Rostamian H et al (2015) Thermal conductivity of Cu/TiO2–water/EG hybrid nanofluid: experimental data and modeling using artificial neural network and correlation. Int Commun Heat Mass Transf 66:100–104. https://doi.org/10.1016/j.icheatmasstransfer.2015.05.014
30. Shukla KN, Brusly Solomon A, Pillai BC, Jacob Ruba Singh B, Saravana Kumar S (2012) Thermal performance of heat pipe with suspended nano-particles. Heat Mass Transf 48(11):1913–1920. https://doi.org/10.1007/s00231-012-1028-4
31. Yiamsawas T, Mahian O, Dalkilic AS, Kaewnai S, Wongwises S (2013) Experimental studies on the viscosity of TiO_2 and Al_2O_3 nanoparticles suspended in a mixture of ethylene glycol and water for high temperature applications. Appl Energy 111:40–45. https://doi.org/10.1016/j.apenergy.2013.04.068
32. Timofeeva EV (2011) Nanofluids for heat transfer—POTENTIAL AND ENGINEERING STRATEGIES. In: Ahsan A (ed) Two Phase Flow, Phase Change and Numerical Modelling. InTech, Croatia, pp 435–450
33. Xu J, Bandyopadhyay K, Jung D (2016) Experimental investigation on the correlation between nano-fluid characteristics and thermal properties of Al_2O_3 nano-particles dispersed in ethylene glycol–water mixture. Int J Heat Mass Transf 94: 262–268. https://doi.org/10.1016/j.ijheatmasstransfer.2015.11.056
34. Mashaei PR, Shahryari M, Madani S (2016) Analytical study of multiple evaporator heat pipe with nanofluid; a smart material for satellite equipment cooling application. Aerosp Sci Technol 59:112–121. https://doi.org/10.1016/j.ast.2016.10.018
35. Keshavarz Moraveji M, Razvarz S (2012) Experimental investigation of aluminum oxide nanofluid on heat pipe thermal performance. Int Commun Heat Mass Transf 39(9):1444–1448. https://doi.org/10.1016/j.icheatmasstransfer.2012.07.024
36. Noie SH, Heris SZ, Kahani M, Nowee SM (2009) Heat transfer enhancement using Al_2O_3–water nanofluid in a two-phase closed thermosyphon. Int J Heat Fluid Flow 30(4):700–705. https://doi.org/10.1016/j.ijheatfluidflow.2009.03.001
37. Esfe MH, Hajmohammad MH (2017) Thermal conductivity and viscosity optimization of nanodiamond-Co_3O_4/EG (40:60) aqueous nanofluid using NSGA-II coupled with RSM. J Mol Liq 238:545–552. https://doi.org/10.1016/j.molliq.2017.04.056
38. Hemmat Esfe M, Abbasian Arani AA, Shafiei Badi R, Rejvani M (2018) ANN modeling, cost performance and sensitivity analyzing of thermal conductivity of DWCNT–SiO_2/EG hybrid nanofluid for higher heat transfer. J Therm Anal Calorim 131(3):2381–2393. https://doi.org/10.1007/s10973-017-6744-z
39. Shanbedi M, Zeinali Heris S, Maskooki A, Eshghi H (2015) Statistical analysis of laminar convective heat transfer of MWCNT-deionized water nanofluid using the response surface methodology. Num Heat Transf Part A 68:454–469.
40. Vajjha RS, Das DK (2015) An experimental determination of the viscosity of propylene glycol/water based nanofluids and development of new correlations. Int J Mat Sci Eng 356-387:98–128
41. Hemmat EM, Hassani AMR, Toghraie D, Hajmohammad MH, Rostamian H, Tourang H (2016) Designing artificial neural network on thermal conductivity of Al_2O_3–water–EG (60–40%) nanofluid using experimental data. J Therm Anal Calorim 126(2):837–843. https://doi.org/10.1007/s10973-016-5469-8
42. Heris SZ, Edalati Z, Noie SH, Mahian O (2014) Experimental investigation of Al_2O_3/water nanofluid through equilateral triangular duct with constant wall heat flux in laminar flow. Heat Transf Eng 35(13):1173–1182. https://doi.org/10.1080/01457632.2013.870002
43. Wang PY, Chen XJ, Liu ZH, Liu YP (2012) Application of nanofluid in an inclined mesh wicked heat pipes. Thermochim Acta 539:100–108. https://doi.org/10.1016/j.tca.2012.04.011
44. Solomon AB, Ramachandran K, Pillai BC (2012) Thermal performance of a heat pipe with nanoparticles coated wick. Appl Therm Eng 36(1):106–112. https://doi.org/10.1016/j.applthermaleng.2011.12.004
45. Vijayakumar M, Navaneethakrishnan P, Kumaresan G (2016) Thermal characteristics studies on sintered wick heat pipe using CuO and Al_2O_3 nanofluids. Exp Thermal Fluid Sci 79:25–35. https://doi.org/10.1016/j.expthermflusci.2016.06.021
46. Suresh Kumar B, Baskar N (2013) Integration of fuzzy logic with response surface methodology for thrust force and surface roughness modeling of drilling on titanium alloy. Int J Adv Manuf Technol 65(9-12):1501–1514. https://doi.org/10.1007/s00170-012-4275-0

Publisher's Note